Black Sea Journal of Engineering and Science
doi: 10.34248/bsengineering.1663812

Open Access Journal
e-ISSN: 2619 – 8991

Research Article
Volume 8 - Issue 5: XX-XX / September 2025

EFFECT OF SOIL-STRUCTURE INTERACTION ON THE TORSIONAL BEHAVIOR OF L-SHAPED RC BUILDINGS UNDER BI-DIRECTIONAL GROUND MOTIONS

Ibrahim OZ[1]*

[1]*Kirsehir Ahi Evran University, Faculty of Engineering and Architecture, Department of Civil Engineering, 40100, Kirsehir, Türkiye*

Abstract: This study investigates the seismic torsional response of a nine-story L-shaped reinforced concrete (RC) building, with particular emphasis on the effects of soil-structure interaction (SSI). Using three-dimensional nonlinear dynamic analyses in SAP2000, the building's performance was evaluated under 30 pairs of scaled bidirectional ground motion records. SSI effects were modeled using the substructure method, with soil properties corresponding to ZC soil class as defined by the Turkish Seismic Code (TBEC-2018). Torsional behavior coefficients (ηbi) were computed from the displacement differentials obtained, and fragility curves were developed using ηbi as the engineering demand parameter. The results showed that SSI increased the fundamental periods by approximately 8% and torsional irregularity by up to 30% compared to fixed-base conditions. Fragility analysis indicated that the probability of exceeding the critical ηbi value of 1.2 was approximately 10% under fixed-base conditions and about 40% when SSI was considered. These findings highlight the significant impact of SSI on the torsional response of irregular structures and emphasize the importance of accounting for SSI effects in the seismic design and performance assessment of RC buildings.

Keywords: Torsional irregularity, Soil-structure interaction, Nonlinear dynamic analysis, Fragility curve, L-shaped building.

***Corresponding author:** Kirsehir Ahi Evran University, Faculty of Engineering and Architecture, Department of Civil Engineering 40100, Kirsehir, Türkiye.
E mail: ibrahim.oz@ahievran.edu.tr (I. OZ)
Ibrahim OZ https://orcid.org/ 0000-0003-3152-3675

Received: March 23, 2025
Accepted: June 11, 2025
Published: September 15, 2025

Cite as: Oz İ, 2025. Effect of soil-structure interaction on the torsional behavior of l-shaped RC buildings under bi-directional ground motions. BSJ Eng Sci, 8(5): xx-xx.

1. Introduction

Recent severe earthquakes, particularly those occurring in our country, have underscored the necessity for reinforced concrete (RC) buildings to exhibit sufficient resistance under seismic loads. To achieve desirable seismic performance during earthquakes, RC structures must possess essential attributes such as adequate lateral strength, stiffness, and ductility (Abdel Raheem et al., 2018). Consequently, the plan layout of an RC building plays a critical role in its design under seismic loading. Regulatory provisions specifying the requirements for RC structures constitute the most crucial criteria for ensuring seismic resilience (Abdel Raheem et al., 2010). Although RC frames with regular structural configurations are comparatively easier to design and predict in terms of seismic response, architectural considerations and site-specific constraints often preclude the feasibility of uniformly regular structural layouts (Abdel Raheem et al., 2018).

In practical scenarios, almost all structures exhibit some form of irregularity, rendering torsional coupling effects unavoidable under seismic excitation (Sucuoglu and Kaatsiz, 2021). For engineers designing irregular buildings in regions with high seismicity, ensuring structural safety is the paramount objective (Solomon and Hemalatha, 2013, Ozer and Inel, 2025). Particularly for L-shaped buildings, asymmetrical distributions of mass, stiffness, and strength arising from plan irregularities frequently exceed the rotational and translational limits defined by seismic codes, potentially resulting in significant damage. Additionally, re-entrant corners and lateral-torsional coupling can substantially amplify seismic demands on the structure. Therefore, the design of structural elements within irregular regions requires meticulous attention (Abdel Raheem et al., 2018). Field investigations conducted following major earthquakes have highlighted increased damage rates in irregular structures (De Stefano and Pintucchi 2008) and (Das et al (2021). Consequently, the design and seismic performance assessment of RC buildings exhibiting torsional effects become considerably more complex compared to symmetric buildings (Sucuoglu and Kaatsiz, 2021; Abdel Raheem et al., 2018).

In recent years, advancements in computational software and engineering knowledge have accelerated research on soil-structure interaction (SSI). Numerous studies in the literature have demonstrated that incorporating SSI significantly alters the dynamic response of structures, particularly affecting their fundamental vibration periods Najar et al. (2025), Brathi et al. (2025) and increasing story drifts (Shirzadi, 2020). Although the necessity of utilizing torsionally irregular buildings underscores the importance of studying the combined influence of SSI and torsional behavior, there remains a notable gap in the literature regarding such investigations. This study addresses this gap by analyzing the torsional irregularity of a nine-story L-shaped RC building, comparing its response under both fixed-base conditions and considering SSI effects. The findings indicate that incorporating SSI can increase torsional irregularity by up to 30%, emphasizing the importance of considering SSI effects in both the design and evaluation of RC buildings.

2. Materials and Methods

2.1. Structure and SSI model

In this study, a reinforced concrete building with a simple L-type frame structure was used, having a total height of 29.9 m, with the first-floor height at 3.5 m and each of the remaining 8 floors at 3.3 m. Reinforced concrete columns were selected with dimensions of 60x60 cm, while beam dimensions were considered as 25x50 cm. According to the Turkish Earthquake Code, the structure's importance factor was taken as 1, and the seismic load reduction factor was selected as 8. During the modeling phase, walls and slabs were not individually modeled but were incorporated only as loads. Dead and live loads were chosen as 5 kN/m, while wall loads were set as 3.25 kN/m. Cross-section stiffness values were defined as 0.7EI for columns and 0.35EI for beams in accordance with TBEC-2018. In the study, concrete compressive strength was considered as 30 MPa, reinforcement yield strength as 420 MPa, and transverse reinforcement spacing in confinement regions was set at 10 cm. The foundation of the building was modeled using frame elements with a depth of 80 cm.

Three-dimensional structural models were developed using SAP2000, a widely recognized structural analysis software for dynamic assessments. To accurately capture the nonlinear behavior of frame structural members, lumped fiber-hinge elements were employed, with hinges directly defined based on material nonlinearity. Each hinge was modeled using fiber elements, with stiffness derived directly from the nonlinear characteristics of the material. According to (Carvalho et al 2013)., a single hinge at each member end is sufficient to simulate biaxial bending, and the hinge length was set at 0.5 times the section height. The structural axis spans were selected as 5 meters, resulting in a total span of 50 meters in both directions, and the ratio of the non-irregular part to the L-shaped arms was considered as 4. A visual representation of the three-dimensional computer model of the structure is presented in Figure 1.

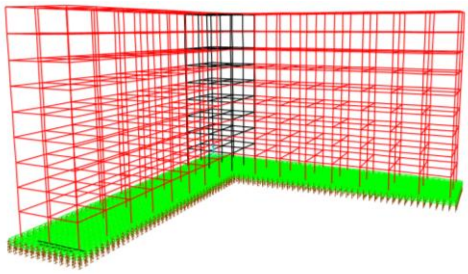

Figure 1. Three-dimensional view of the modeled L-type building.

In the study, the substructure method was used to avoid the computational load imposed by the direct method. A comparison of substructure method with the direct method was conducted in the study by (Oz, 2025). In the method under consideration, the surface stiffness values are to be multiplied by the embedment effects, and the radiation damping for embedded footings is given by the formulas presented in Table 1. The arrangement of the springs at the foundation level is illustrated in Figure 2 and Figure 3.

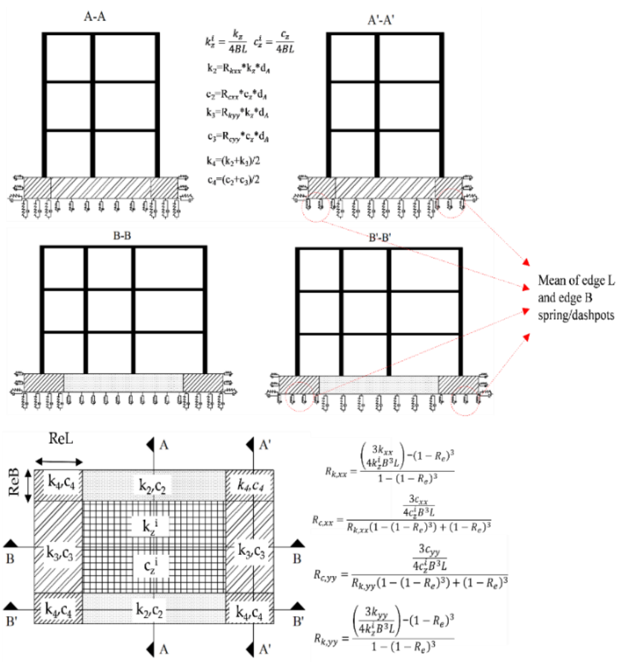

Figure 2. SSI Modeling: stiffness and damping expressions for raft foundation systems.

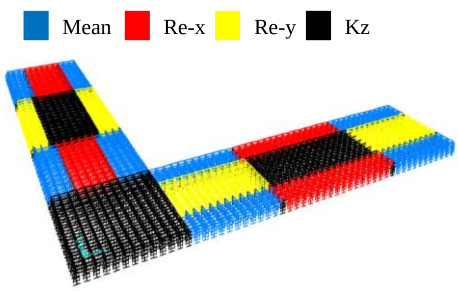

Figure 3. Spring groups and their layout used in the L-shaped building.

Table 1. The formulas used for calculating soil springs

Radiation Damping Ratios for Embedded Footings	Elastic Solutions for Static Stiffness of Rigid Footings at the Ground Surface
$\beta_z = \left[\frac{4[\psi(L/B) + (D/B)(1 + L/B)]}{(K_{z,emb}/GB)}\right]\left[\frac{a_0}{2\alpha_z}\right]$	$K_{z,\,\mathrm{sur}} = \frac{GB}{1-v}\left[3.1\left(\frac{L}{B}\right)^{0.75} + 1.6\right]$
$\beta_y = \left[\frac{4[L/B + (D/B)(1 + \psi L/B)]}{(K_{y,emb}/GB)}\right]\left[\frac{a_0}{2\alpha_y}\right]$	$K_{y,\,\mathrm{sur}} = \frac{GB}{2-v}\left[6.8\left(\frac{L}{B}\right)^{0.65} + 0.8\left(\frac{L}{B}\right) + 1.6\right]$
$\beta_x = \left[\frac{4[L/B + (D/B)(\psi + L/B)]}{(K_{x,emb}/GB)}\right]\left[\frac{a_0}{2\alpha_x}\right]$	$K_{x,\,\mathrm{sur}} = \frac{GB}{2-v}\left[6.8\left(\frac{L}{B}\right)^{0.65} + 2.4\right]$
$\beta_{zz} = \left[\frac{(4/3)[3(L/B)(D/B) + \psi(L/B)^3(D/B) + 3(L/B)^2(D/B) + \psi(D/B) + (L/B)^3 + (L/B)]a_0^2}{\left(\frac{K_{zz,emb}}{GB^3}\right)\left[\left(\frac{1.4}{1+3(L/B-1)^{0.7}}\right) + a_0^2\right]}\right]\left[\frac{a_0}{2\alpha_{zz}}\right]$	$K_{zz,sur} = GB^3\left[4.25\left(\frac{L}{B}\right)^{2.45} + 4.06\right]$
$\beta_{yy} = \left[\frac{(4/3)\left[\left(\frac{L}{B}\right)^3\left(\frac{D}{B}\right) + \psi\left(\frac{D}{B}\right)^3\left(\frac{L}{B}\right) + \left(\frac{D}{B}\right)^3 + 3\left(\frac{D}{B}\right)\left(\frac{L}{B}\right)^2 + \psi\left(\frac{L}{B}\right)^3\right]a_0^2}{\left(\frac{K_{yy,emb}}{GB^3}\right)\left[\left(\frac{1.8}{1+1.75(L/B-1)}\right) + a_0^2\right]} + \frac{\left(\frac{4}{3}\right)\left(\frac{L}{B} + \psi\right)\left(\frac{D}{B}\right)^3}{\left(\frac{K_{yy,emb}}{GB^3}\right)}\right]\left[\frac{a_0}{2\alpha_{yy}}\right]$	$K_{yy,sur} = \frac{GB^3}{1-v}\left[3.73\left(\frac{L}{B}\right)^{2.4} + 0.27\right]$
$\beta_{xx} = \left[\frac{(4/3)\left[\left(\frac{D}{B}\right) + \left(\frac{D}{B}\right)^3 + \psi\left(\frac{L}{B}\right)\left(\frac{D}{B}\right)^3 + 3\left(\frac{D}{B}\right)\left(\frac{L}{B}\right) + \psi\left(\frac{L}{B}\right)\right]a_0^2}{\left(\frac{K_{xx,emb}}{GB^3}\right)\left[\left(\frac{1.8}{1+1.75(L/B-1)}\right) + a_0^2\right]} + \frac{\left(\frac{4}{3}\right)\left(\psi\frac{L}{B} + 1\right)\left(\frac{D}{B}\right)^3}{\left(\frac{K_{xx,emb}}{GB^3}\right)}\right]\left[\frac{a_0}{2\alpha_{xx}}\right]$	$K_{\mathrm{xx},\,\mathrm{sur}} = \frac{GB^3}{1-v}\left[3.2\left(\frac{L}{B}\right) + 0.8\right]$

While calculating the springs representing the soil medium used in the study, the guidelines from the National Institute of Standards 2012– Soil-Structure Interaction for Building Structures – were utilized (NIST, 2012). The unit weight of the considered soil was taken as 20 kN/m^3, the shear wave velocity as 400 m/s, and the Poisson's ratio as 0.3. The modeled soil corresponds to ZC soil class according to TBEC-2018 (TBEC-2018). The first three modes of the analyzed L-type building for both fixed-base (FB) and ZC (SSI) conditions are presented in Table 2. The flexural behavior of the foundation was considered in the analysis to more accurately reflect its realistic response (OZ, 2025).

2.2. Selection of ground motions

In the study, it was assumed that the L-type building is located in Hatay, and the coordinates were selected as latitude 36.20^0 and longitude 36.15^0 using the Türkiye Earthquake Hazard Maps Interactive Web Application. The seismic ground motion level was selected as Design Basis Earthquake, and the local soil class was chosen as ZC, which corresponds to the soil type considered in the study, to determine the design spectrum.

A total of 30 acceleration records were selected from the PEER (PEER, 2021) Strong Ground Motion Database in accordance with the considered V_{s30} value. The SRSS spectra of the selected records, their average spectrum, and the determined target spectrum are presented in Figure 4. The parameters of the selected records are shown in Table 3.

Table.2 Period elongations by SSI effects

Model	Mode 1 (sec)	Mode 2 (sec)	Mode 1 (sec)
FB	1.671	1.592	1.515
SSI	1.827	1.711	1.629
Elongation Ratio (%)	8.54	6.95	7.00

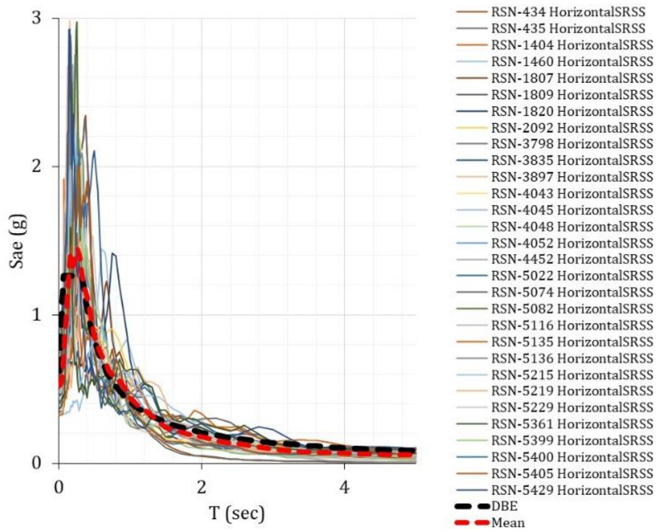

Figure 4. Elastic acceleration spectrum of the scaled records for 5 % damping.

Table.3 Ground motion properties used in the study

Record Sequence Number	Magnitude	Rjb (km)	Vs30 (m/sec)	PGA
434	6.88	100.220	445.660	2.344
435	6.88	100.220	445.660	2.317
1404	7.62	110.300	465.860	2.148
1460	7.62	114.280	429.490	1.444
1807	7.13	146.510	442.020	1.487
1809	7.13	112.260	414.030	1.424
1820	7.13	171.890	430.690	1.417
2092	6.70	119.840	424.900	1.527
3798	7.13	177.390	418.830	1.433
3835	7.90	139.110	428.080	2.106
3897	6.61	101.340	481.500	2.983
4043	6.60	190.890	477.350	2.190
4045	6.60	104.820	441.840	1.670
4048	6.60	133.300	412.230	2.184
4052	6.60	155.460	477.350	2.227
4452	7.10	118.210	485.040	2.749
5022	6.80	147.650	431.940	1.432
5074	6.80	134.370	467.350	2.889
5082	6.80	131.500	406.760	2.973
5116	6.80	106.860	487.670	1.477
5135	6.80	182.610	440.000	1.554
5136	6.80	158.140	427.040	2.314
5215	6.80	195.890	478.540	2.004
5219	6.80	131.020	432.690	1.488
5229	6.80	146.600	473.500	1.586
5361	6.80	141.960	423.000	1.592
5399	6.80	125.850	471.230	2.065
5400	6.80	159.010	461.740	2.090
5405	6.80	158.820	425.880	2.006
5429	6.80	142.100	471.420	2.928

3. Results and Discussion

In this study, the Newmark-beta method (Newmark, 1959) was employed for time-history analysis. To ensure unconditional stability, the gamma (γ) and beta (β) coefficients were set to 0.5 and 0.25, respectively. Rayleigh damping was used to formulate the damping, and the damping ratio was assumed to be 5%. The mass and stiffness proportional coefficients were determined based on different period values, and were considered for viscous proportional damping. When determining the number of modes considered in this study, it was ensured that the mass participation rate of the modes exceeded 95%, which corresponds to the first 12 modes for this study.

The torsional behavior coefficients (⍰$_{bi}$) obtained from Nonlinear Dynamic Time History Analyses performed in both the x and y directions for 30 acceleration records will be discussed in this section. Within the scope of the study, only the torsional behavior of a 9-story reinforced concrete building was considered. While calculating the torsional behavior coefficients, the ends of the L-shaped arms and the corner of the building were taken into account. The points where the torsional behavior was considered are shown in Figure 5.

After determining the minimum (⍰$_{imin}$) and maximum (⍰$_{imax}$) displacements per story as specified in the code from the displacements obtained from the nonlinear dynamic time history analyses, the averages (⍰$_{iaverage}$) of these displacements were calculated, and the torsional behavior coefficient was computed separately for each story. These expressions are given by ⍰$_{iaverage}$ in Eq. 1, and the story torsional behavior coefficient ⍰$_{bi}$ is calculated using equation. 2.

$$\Delta_{iaverage} = \frac{\Delta_{imax} - \Delta_{imin}}{2} \tag{1}$$

$$\eta_{bi} = \frac{\Delta_{imax}}{\Delta_{iaverage}} \tag{2}$$

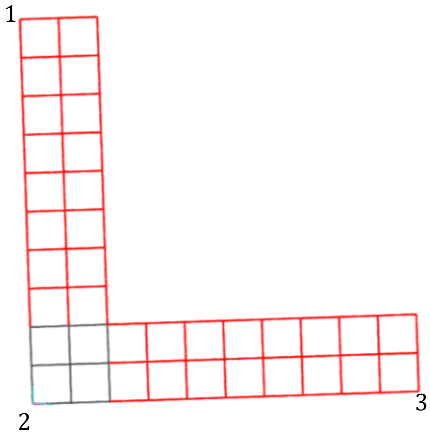

Figure 5. Considered corner points of L shape structure.

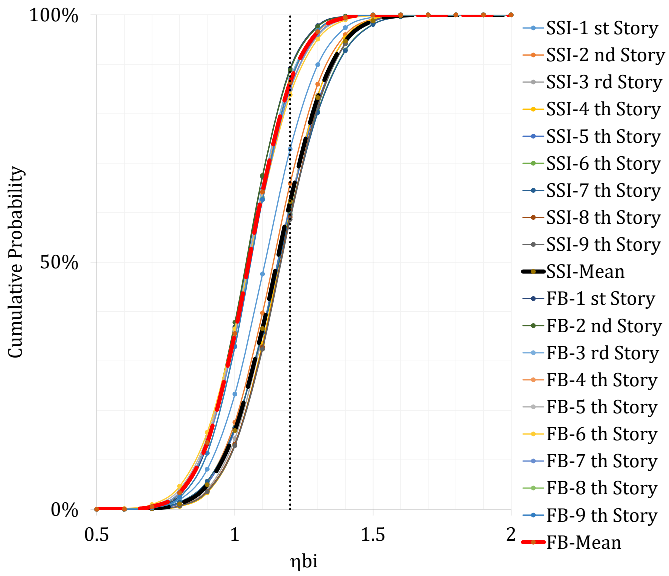

Figure 6. Fragility curves for torsional irregularity.

The fragility curves presented in Figure 6 are developed using a lognormal cumulative distribution function (CDF) to estimate the probability of exceeding specific damage states, with the torsional behavior coefficient (η_{bi}) used as the engineering demand parameter (EDP) (Forcellini, 2021). The fragility function is formulated based on Eq. (3), and the probabilities of exceedance for isolator displacements are also illustrated in Figure 4.

$$\mathrm{P(D > s \mid IM\,)} = \Phi\frac{\ln(IM) - \ln(\mu)}{\sigma} \tag{3}$$

In this context:

P represents the probability of structural damage (D) exceeding a given damage state;

Φ denotes the standard normal cumulative distribution function;

IM is the selected intensity measure value;

σ is the standard deviation of the natural logarithm of the seismic intensity measure;

μ is the mean of the natural logarithm of the seismic intensity measure.

4. Conclusions

In this study, nonlinear time history analyses were performed using 30 different bi-directional ground motion pairs by applying two horizontal components simultaneously, to evaluate the torsional behavior of a nine-story L-shaped reinforced concrete building under seismic loading. The analyses were conducted for both fixed-base and soil-structure interaction (SSI) conditions. Torsional behavior coefficients (ηbi) were calculated for each story based on the displacements obtained from these analyses. Fragility curves developed using ηbi as the engineering demand parameter showed that the probability of exceeding the critical ηbi value of 1.2 was approximately 10% for the fixed-base condition and about 40% under SSI. These observations clearly demonstrate the significant influence of SSI on torsional response and highlight the importance of accounting for SSI effects in the seismic design and performance assessment of torsionally irregular structures.

Author Contributions

The percentages of the author's contributions are presented below. The author reviewed and approved the final version of the manuscript.

	I. O.
C	100
D	100
S	100
DCP	100
DAI	100
L	100
W	100
CR	100
SR	100
PM	100
FA	100

C=Concept, D= design, S= supervision, DCP= data collection and/or processing, DAI= data analysis and/or interpretation, L= literature search, W= writing, CR= critical review, SR= submission and revision, PM= project management, FA= funding acquisition.

Conflict of Interest

The author declared that there is no conflict of interest.

Ethical Consideration

Ethics committee approval was not required for this study because of there was no study on animals or humans.

References

Abdel Raheem KA, Abdel Raheem SE, Soghair HM, Ahmed MH, 2010. Evaluation of seismic performance of multistory buildings designed according to Egyptian code. J Eng Sci Assiut Univ 38(2): 381-402.

Abdel Raheem SE, Ahmed MM, Ahmed MM, Abdel-shafy AG. 2018. Evaluation of plan configuration irregularity effects on seismic response demands of L-shaped MRF buildings. Bull Earthq Eng 16: 3845-3869.

Bharti AK, Garg V, Chandrawanshi S. 2025. A critical review of seismic soil-structure interaction analysis. J Istruc 72: 108221.

Carvalho G, Bento R, Bhatt C. 2013. Nonlinear static and dynamic analyses of reinforced concrete buildings—Comparison of different modelling approaches. Earthq Struct 4(5): 451-470.

Das PK, Dutta SC, Datta TK. 2021. Seismic behavior of plan and vertically irregular structures: state of art and future challenges. Nat Hazards Rev 22(2): 04020062.

De Stefano M, Pintucchi B. 2008. A review of research on seismic behaviour of irregular building structures since 2002. Bull Earthq Eng 6: 285-308.

Forcellini D. 2021. Analytical fragility curves of shallow-founded structures subjected to soil-structure interaction (SSI) effects. Soil Dyn Earthq Eng 141: 106487.

Najar IA, Ahmadi R, Amuda AG, Mourad R, Bendary NE, Ismail I, Tang S. 2025. Advancing soil-structure interaction (SSI): a comprehensive review of current practices, challenges, and future directions. J Infrastruct Preserv Resil 6(1): 5.

Newmark NM. 1959. A method of computation for structural dynamics. J Eng Mech Div 85(3): 67-94.

NIST G. 2012. Soil-structure interaction for building structures. National Earthquake Hazards Reduction Program (NEHRP), pp: 1-20.

Oz I. 2025. Seismic pounding effects of typical midrise reinforced concrete structures subjected to soil–structure interaction effects. J Steng 151(2): 05024005.

Ozer E, Inel M. 2025. The effect of single and combined use of base isolator and fluid viscous damper on seismic performance in a conventional RC building with torsional irregularity. J Build Eng 101: 111898.

PEER. Pacific Earthquake Engineering Research Center. Strong ground motion database (accessed date: November, 2024). https://ngawest2.berkeley.edu/

Shirzadi M, Behnamfar F, Asadi P. 2020. Effects of soil–structure interaction on inelastic response of torsionally-coupled structures. Bull Earthq Eng 18: 1213-1243.

Solomon AA, Hemalatha G. 2013. Limitation of irregular structure for seismic response. Int J Civil Struct Eng 3(3): 579-590.

Sucuoğlu H, Kaatsız K. 2021. Torsional ductility spectrum for predicting ductility distribution in simple asymmetric-plan structures. Earthq Eng Struct Dyn 50(2): 538-559.

TBEC. 2018. Turkish Seismic Earthquake Code, pp: 1-416.